Accepted Manuscript

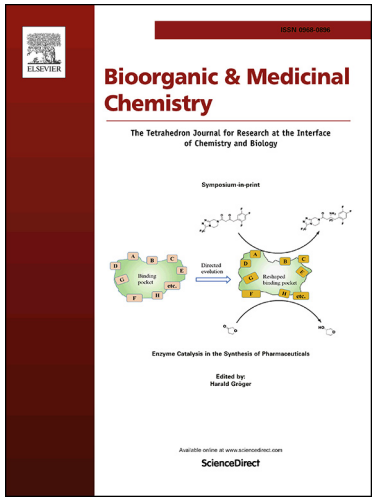

Design, synthesis and structure-activity relationship of diaryl-ureas with novel isoxazol[3,4-*b*]pyridine-3-amino-structure as multi-target inhibitors against receptor tyrosine kinase

Zhi-Hao Shi, Feng-Tao Liu, Hao-Zhong Tian, Yan-Min Zhang, Nian-Guang Li, Tao Lu

PII: S0968-0896(18)31350-6
DOI: https://doi.org/10.1016/j.bmc.2018.08.013
Reference: BMC 14500

To appear in: *Bioorganic & Medicinal Chemistry*

Received Date: 25 July 2018
Revised Date: 9 August 2018
Accepted Date: 10 August 2018

Please cite this article as: Shi, Z-H., Liu, F-T., Tian, H-Z., Zhang, Y-M., Li, N-G., Lu, T., Design, synthesis and structure-activity relationship of diaryl-ureas with novel isoxazol[3,4-*b*]pyridine-3-amino-structure as multi-target inhibitors against receptor tyrosine kinase, *Bioorganic & Medicinal Chemistry* (2018), doi: https://doi.org/10.1016/j.bmc.2018.08.013

Design, synthesis and structure-activity relationship of diaryl-ureas with novel isoxazol[3,4-*b*]pyridine-3-amino-structure as multi-target inhibitors against receptor tyrosine kinase

Zhi-Hao Shi[a], Feng-Tao Liu[a], Hao-Zhong Tian[a], Yan-Min Zhang[a], Nian-Guang Li[b,*], Tao Lu[a,*]

[a]School of Science, China Pharmaceutical University, 639 Longmian Avenue, Nanjing, Jiangsu 211198, China

[b]National and Local Collaborative Engineering Center of Chinese Medicinal Resources Industrialization and Formulae Innovative Medicine, Nanjing University of Chinese Medicine, 138 Xianlin Road, Nanjing, Jiangsu 210023, China

* Corresponding author.

E-mail addresses: linianguang@njucm.edu.cn (N.-G. Li), lutao@cpu.edu.cn (T. L)

ABSTRACT

Inspired by that the multi-target inhibitors against receptor tyrosine kinases (RTKs) have significantly improved the effect of clinical treatment for cancer, and based on the chemical structure of Linifanib (ABT-869, Abbott), two series of diaryl-ureas with novel isoxazol[3,4-*b*]pyridine-3-amino-structure were designed and synthesized as multi-target inhibitors against RTKs. The preliminary biological evaluation showed that several compounds exhibited comparable potency with Linifanib. Compound **S21** was identified as the most potent inhibitor against Fms-like tyrosine kinase 3 (FLT-3), kinase insert domain containing receptor (KDR) and platelet-derived growth factor receptor β (PDGFR-β) with its IC_{50} values were 4 nM, 3 nM and 8 nM respectively, it also showed potent inhibitory activities against several caner cells.

Keywords: Multi-target inhibitors, receptor tyrosine kinase, FLT3, KDR, PDGFR-β, antiangiogenesis

1. Introduction

Cancer is one of challenging field for medicinal chemists to discover effective yet safer chemotherapeutic agents targeting various biochemical processes involved in progression of cancers.[1] Angiogenesis, the formation of new capillaries from the endothelium of an existing vascular network, plays a crucial role in tumor growth. Angiogenesis is involved in metastasis (uncontrolled spread of tumor cells) by supplying oxygen, nutrients, and related growth factors to small tumors and removing the waste products of metabolism. Solid tumors cannot grow beyond several cubic millimeters until they establish a blood supply because cells must be within 100–200 μm of a blood vessel to survive.[2]

Receptor tyrosine kinases (RTKs) have been shown not only to be key regulators of normal cellular processes, but also to have a critical role in the development and progress of cancers. RTKs play fundamental roles in transformation, proliferation, migration, differentiation and metastasis of cancer cells.[3] At least 19 RTK subfamilies have been identified. One example is the platelet-derived growth factor receptor (PDGFR) subfamily. Members of this family include PDGFR-α, PDGFR-β, colony-stimulating factor-1 receptor (CSF-1R), Fms-like tyrosine kinase 3 (FLT-3) and c-KIT. These kinases are believed to promote angiogenesis and tumor cell growth.

All RTKs share a similar molecular architecture, including a ligand binding extracellular region, a single transmembrane helix, an intracellular regulatory domain, and a cytoplasmic tyrosine kinase domain.[4] The ATP-binding site of RTK shares remarkable sequence homology and structural resemblance with each other such as epidermal growth factor receptor (EGFR), kinase insert domain containing receptor (KDR) and fibroblast growth factor receptor 1 (FGFR1). All these information provides a possibility for the design of multi-target inhibitors against RTKs. The clinical application of multi-target RTK inhibitors has been validated as a therapeutic strategy by positive results with Sorafenib (BAY-43-9006, Bayer), Vandetanib (ZD6474, AstraZeneca), Sunitinib (SU-11248, Pfizer) and Linifanib (ABT-869, Abbott) (Fig. 1).[5]

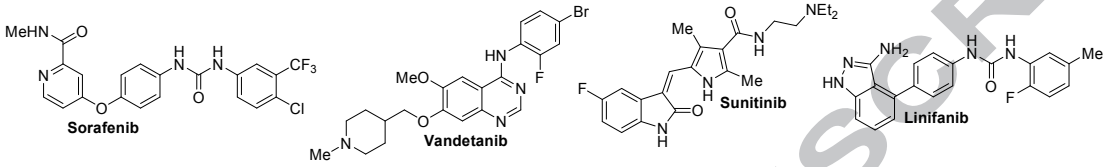

Figure 1. Structures of multi-target receptor tyrosine kinase inhibitors

Sorafenib (BAY-43-9006, Bayer) is a small molecular inhibitor of several RTKs (VEGFR/PDGFR/ERK) and Raf kinases, approved for the treatment of primary kidney cancer (advanced renal cell carcinoma), advanced primary liver cancer (hepatocellular carcinoma), and radioactive iodine resistant advanced thyroid carcinoma.[6] Vandetanib (ZD6474, AstraZeneca) is an anti-cancer drug that is used for the treatment of certain tumors of the thyroid gland, it acts as a kinase inhibitor of a number of cell receptors (VEGFR/EGFR/RET-tyrosine kinase).[7] Sunitinib (SU11248, Pfizer) is an oral, small-molecule, multi-targeted RTK inhibitor of PDGF-Rs/VEGFRs/c-KIT for the treatment of renal cell carcinoma (RCC) and imatinib-resistant gastrointestinal stromal tumor (GIST).[8] Linifanib (ABT-869, Abbott) is an oral active multi-target RTK inhibitor of KDR, PDGFR-β and CSF-1R, the phase II trial studies shows that Linifanib works well in treating patients with advanced, refractory colorectal cancer expressing k-Ras mutations.[9]

Recently, many researches have highlighted diarylureas as potential antiproliferative agents,[10] and Linifanib has attracted considerable attention. In this study, we selected *N*,*N*'-diarylurea as core structure to obtain novel multi-target RTK inhibitors,[11] and we took Linifanib as our lead compound because it could inhibit FLT-3, VEGFR-2 and PDGFR-β with its IC_{50}s were 4 nM, 4 nM and 66 nM respectively.[12]

The structure–activity relationship (SAR) of Linifanib (Fig. 2) indicated that 3-aminoindazole[13] could serve as an efficient hinge-binding template for kinase inhibitors, and 3-methyl-pyrazolo[3,4-*b*] pyridine core scaffold[14] was also a good pharmacophore of the c-KIT/PDGFRα dual inhibitor. By incorporating the *N,N'*-diaryl urea moiety at the above pharmacophore, the RTK inhibitors were generated, which potently inhibited the tyrosine kinase activity of the vascular endothelial growth factor receptor and the platelet-derived growth factor receptor families. The urea linker with lone linear alkyl group and terminal *N*-substituents, e.g., large fused heteroaryl group, could substantially improve the potency. Unfortunately, the amide, sulfonamide and thiourea linker obviously lost activity against all the kinases (PDGFRα, VEGFR2 and FGFR1).[14]

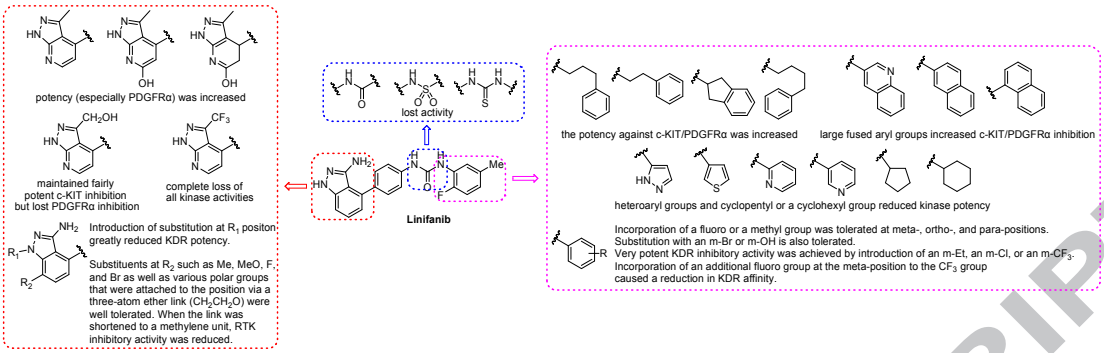

Figure 2. The structure activity relationship of Linifanib.

In order to expand the structural diversity of Linifanib, our design strategy firstly incorporated 3-amino-isoxazol[3,4-b]pyridine to form interaction with ATP-bind site (Fig. 3). Based on the docking studies between Linifanib and **S27** with FLT3 (PDB ID: 4RT7), the 3-aminoindazole in Linifanib could interact with the active sites in FLT3 as the same as 3-amino-isoxazol[3,4-b]pyridine in **S27**. The two nitrogen atoms in 3-aminoindazole in Linifanib, the nitrogen atom and oxygen atom in isoxazole ring of **S27** could form two hydrogen bonds with Cys 694, and the amino group in the two compounds could form a hydrogen bond to Glu 692 in the active hinge region of FLT3. The carbonyl group in urea moiety in Linifanib and **S27** could form one hydrogen bond with Asp 829, and one NH of the urea moiety could form one hydrogen bond with Glu 661. Secondly, we investigated the influence of the terminal aniline which was replaced by other substituted benzene rings, considering its broadly biological activity in anticancer drugs. Furthermore, the substituted acrylamide was also introduced to the target compounds, hoping our target compounds could form irreversible bonds with the kinase, because the irreversible kinase inhibitors show enhanced potency when compared to structurally similar conventional inhibitors, and there is also the expectation that an irreversible inhibitor need not exhibit prolonged circulating blood levels to achieve a desired biological effect.[15] Based on the docking studies, we found that the substituted acrylamide at R_1 position could be in the large hydrophobic pockets formed by Lys644, Met664, Leu668, Val808 and His809. The distance between the β-carbon in the unsaturated amide and the Cys807 was only 4.4Å, it was fit to form a covalent bond.

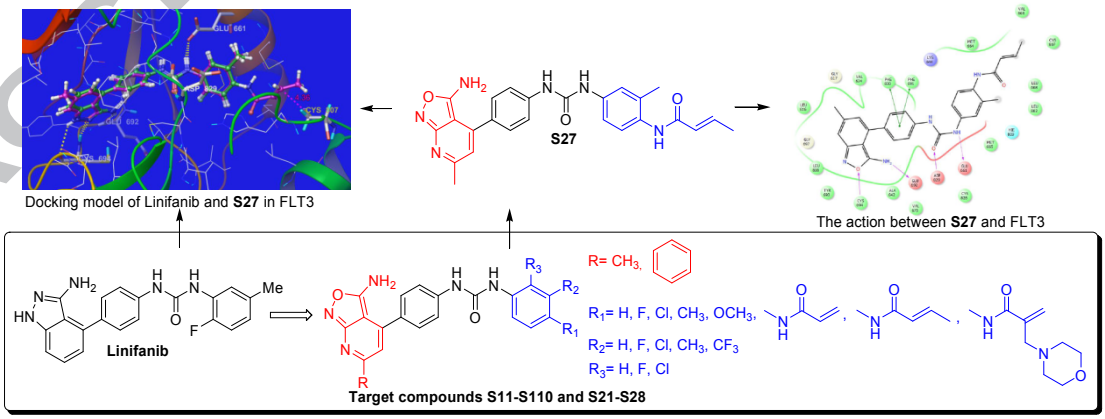

Figure 3. The design of expanding the structural diversity of Linifanib.

2. Results and discussion

2.1. Synthesis

The target compounds were synthesized through two different routes. The series **S11**–**S110** in which the phenyl group was substituted at the isoxazol[3,4-b]pyridine were synthesized as shown in Scheme 1. The Aldol reaction between acetophenone (**1**) and 4-nitro-benzaldehyde (**2**) afforded **3** in 86% yield,[16] and the Michael addition of propanedinitrile to **3** produced **4**.[17] Subsequently, we focused our attention to optimize the reaction condition between **4** and hydroxylamine hydrochloride to produce the important intermediate **5**,[18] when MeOH was selected as solvent, and the molar ration of compound **4**:hydroxylamine hydrochloride:KOH was 1:2:3.12, compound **5** was obtained in 77% yield. After the nitro-group in **5** was reduced to amino by stannous chloride dehydrate, the reaction between **6** and isocyanates (**14a**–**14i**, **18a**) afforded the target compounds **S11**–**S110** in good yield.

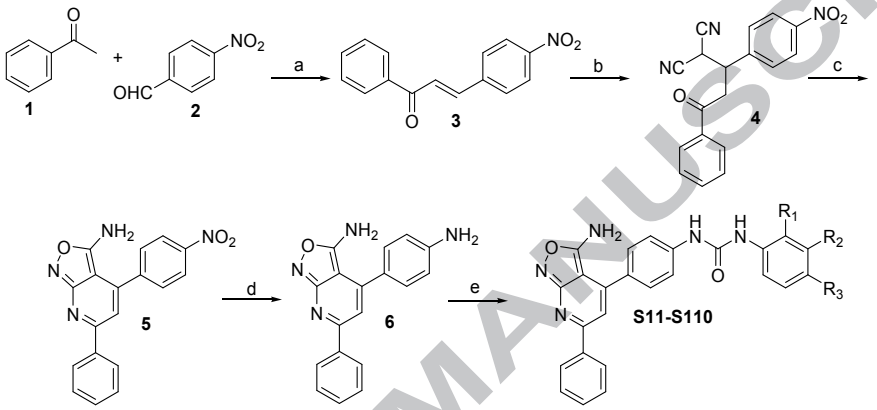

Scheme 1. Reagents and conditions: (a) NaOH, EtOH, 25°C, 24h, 86%; (b) $CH_2(CN)_2$, Bu_3P, DCM, N_2, reflux, 2h, 78%; (c) HO-NH_2·HCl, KOH, MeOH, 0–5°C, 1h, 25°C, 24h, 77%; (d) $SnCl_2·2H_2O$, EtOH, reflux, 89%; (e) Isocyanates (**14a**–**14i**, **18a**), Et_3N, EtOH, 25°C, 2h, 73%–88%.

The series **S21**–**S28** in which the methyl group was substituted at the isoxazol[3,4-b]pyridine were obtained as shown in Scheme 2. The Aldol reaction between 4-nitro-benzaldehyde (**7**) and acetone afforded **8** in 85% yield,[16] then the cyclization between **8** and cyanoacetamide produced **9** in 83% yield.[19] The carbonyl group in **9** was transferred into chlorine by $POCl_3$ to give **10**, then the reduction of nitro group to amino group by iron powder afforded **11**. The second cyclization using **11** and hydroxylamine hydrochloride produced **12** in 69%. Finally, the amino group in **12** reacted with isocyanates (**14a**, **14d**, **14g**, **14k**, **14l**, **18b**, **18c**, **25**) afforded the target compounds **S21**–**S28** in good yield.

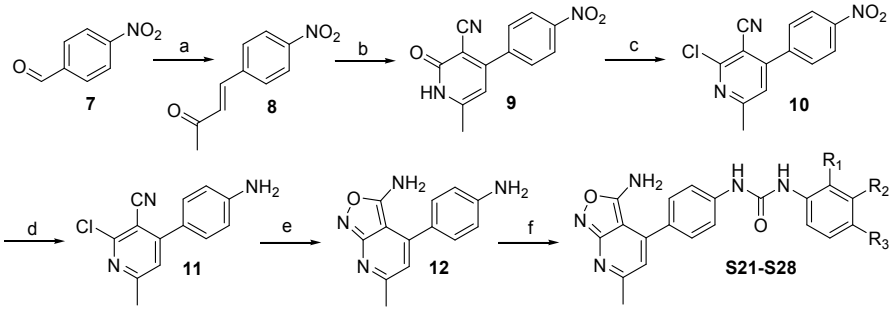

Scheme 2. Reagents and conditions: (a) Acetone, K_2CO_3, 12h, then HCl, 6h, 85%; (b) *t*-BuOK, cyanoacetamide, DMSO, 1h, then *t*-BuOK, air, 2h, 83%; (c) $POCl_3$, reflux, 2h, 77%; (d) Fe, acetic acid, EtOH, reflux, 2h, 89%; (e) HO-NH_2·HCl, *t*-BuOH, reflux, 2h, then *t*-BuOK, reflux, 0.5h, 69%; (f) Isocyanates (**14a**, **14d**, **14g**, **14k**, **14l**, **18b**, **18c**, **25**), Et_3N, EtOH, 25°C, 2h, 65%–82%.

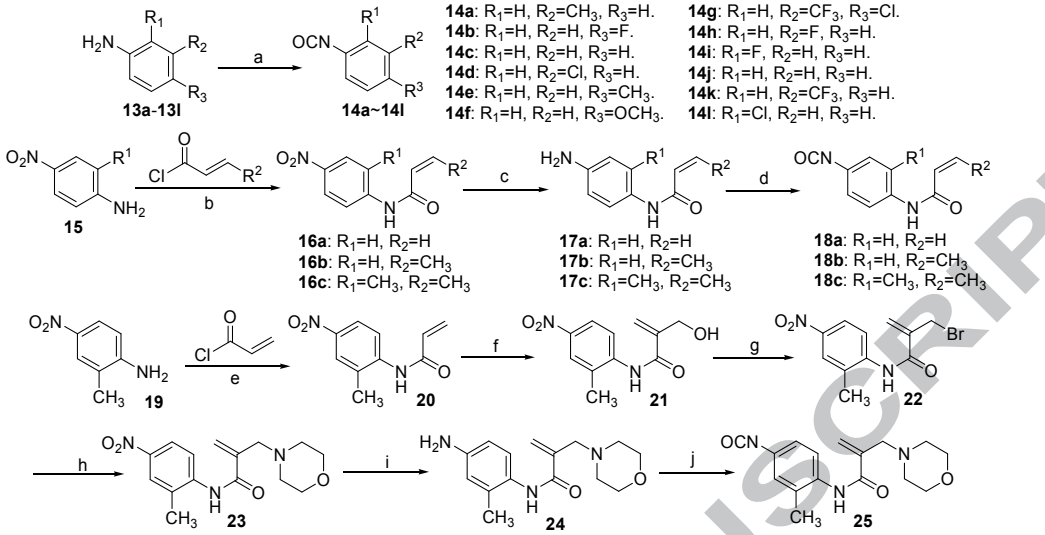

Scheme 3: Reagents and conditions: (a) Triphosgene, EtOAc, 25°C, 1h, then reflux, 4–6h; (b) DIPEA, EtOAc, 25°C, 3h, 85–93%; (c) Fe, EtOH, acetic acid, reflux, 2h, 82–91%; (d) Triphosgene, EtOAc, 0°C, 0.5h, 25°C, 1h, reflux, 4–6h; (e) DIPEA, EtOAc, 25°C, 3h, 85%; (f) paraformaldehyde, DABCO, 1,4-dioxane:H_2O=5:3, 85°C, 8h, 88%; (g) PBr_3, DCM, 25°C, 15min, 84%; (h) morpholine, DCM, 25°C, 15min, 85%; (i) Fe, EtOH, acetic acid, reflux, 93%; (j) Triphosgene, EtOAc, 0°C, 0.5h, 25°C, 1h, reflux, 4h.

The side chains **14a**–**14l**, **18a**–**18c** and **25** were synthesized as shown in Scheme 3. The substituted aniline **13a**–**13l** reacted with triphosgene afforded the isocyanate **14a**–**14l**.[20,21] The reaction between **15a**–**15b** and acroleyl chloride produced the amide derivatives **16a**–**16c**,[22,23] reduction of the nitro group in **16a**–**16c** followed by reaction with triphosgene yielded the substituted isocyanate **18a**–**18c**. The side chain **25** was synthesized from 2-methyl-4-nitrobenzenamine (**19**), reaction of **19** with acroleyl chloride afforded **20** in 85% yield, then the aldol condensation between **20** and paraformaldehyde produced **21**. After the hydroxyl group in **21** was transformed into bromine by PBr_3, the alkylation of **22** to morpholine afforded **23** in 85% yield. At last, the nitro group in **23** was reduced using iron powder, the obtained aniline **24** reacted with triphosgene produced the side chain **25**.

2.2. Biological investigations

2.2.1. Receptor tyrosine kinases inhibitory activities

Table 1 Chemical structures and biological activities of title compounds (IC_{50}, nM)

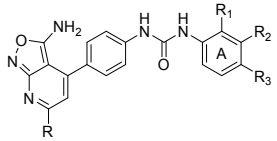

Compd.	R	R_1	R_2	R_3	FLT3	KDR	PDGFR-β
S11		H	CH_3	H	191	130	1230
S12		H	H	F	449	696	3780
S13		H	H	H	1010	NA	3520

S14		H	Cl	H	128	259	2230
S15		H	H	CH_3	311	NA	1260
S16		H	H	OCH_3	177	NA	NA
S17		H	CF_3	Cl	24	685	290
S18		H	F	H	565	105	3250
S19		F	H	H	NA	NA	NA
S110		H	H	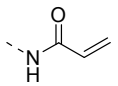	NA	NA	NA
S21	CH_3	H	CH_3	H	4	3	8
S22	CH_3	H	Cl	H	5	25	40
S23	CH_3	H	CF_3	Cl	3	177	20
S24	CH_3	H	CF_3	H	9	11	20
S25	CH_3	Cl	H	H	51	600	820
S26	CH_3	H	H	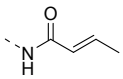	438	NA	NA
S27	CH_3	H	CH_3	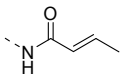	39	NA	NA
S28	CH_3	H	CH_3	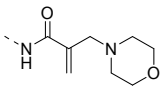	40	167	510
		Linifanib			7	28	60

All the title compounds were evaluated for their enzymatic inhibition against FLT3, KDR and PDGFR-β. The tyrosine kinase inhibitory potency was assayed according to our previous report.[24] The enzymatic inhibitory activity of two series of diarylureas was summarized in Table 1.

For the phenyl substituted isoxazol[3,4-b]pyridine derivatives, compound **S19** with fluorine substituted at the *ortho* position in the A ring showed no inhibitory activity against the three enzymes. When the substitution was introduced at *para* position in the A ring, only **S12** showed inhibitory activity with its IC_{50}s against FLT3, KDR and PDGFR-β were 449 nM, 696 nM and 3780 nM respectively. Furthermore, when the substitution was introduced at *meta* position, three compounds **S11**, **S14** and **S18** showed potent inhibitory activities against FLT3, KDR and PDGFR-β. Interestingly, when the *meta* position and the *para* position were both substituted, the obtained compound **S17** showed the most potent inhibitory activities in this series derivatives, with its IC_{50}s against FLT3 and PDGFR-β were 24 nM and 290 nM. This result suggested that introduction of substitution at *meta* position and the *para* position in ring A of the derivatives was

favorable for their kinases inhibitory activities.

Compounds incorporated with methyl group substituted at the isoxazol[3,4-b]pyridine were generally more potent that those bearing phenyl group. For example, the IC_{50}s against the three enzymes for compound **S22** were 5 nM, 25 nM and 40 nM respectively, while the IC_{50}s for compound **S14** were 128 nM, 259 nM and 2230 nM respectively. When the substitution was introduced at the *para* position in the A ring, compound **S26** lost its inhibitory activity, although its IC_{50} for FLT3 was 438 nM. When the chlorine was introduced at the *ortho* position in the A ring, the obtained compound **S25** showed potent inhibitory activity against the three enzymes, with its IC_{50}s against FLT3, KDR and PDGFR-β were 51 nM, 600 nM and 820 nM respectively. When the chlorine was introduced at the *meta* position in the A ring, compound **S22** showed more potent inhibitory activity than **S25**. The most potent compound was **S21**, with its IC_{50}s against FLT3, KDR and PDGFR-β were 4 nM, 3 nM and 8 nM respectively, while the IC_{50}s of Linifanib against the three enzymes were only 7 nM, 28 nM and 60 nM. Although the compound lost its inhibitory activity when the substitution was introduced at the *para* position at the A ring, when the *para* and the *meta* positions were both substituted, compound **S28** still showed potent inhibitory activity against the three enzymes, with its IC_{50}s were 40 nM, 167 nM and 510 nM respectively. This result confirmed that introduction of substitution at *meta* position in ring A was favorable for the activity.

Unfortunately, compounds **S110**, **S26**, **S27** and **S28** with substituted acrylamide were less potent activities than the other derivatives against the three enzymes, this might be that these compounds did not form irreversible bonds with the kinase.

2.2.2. Antiproliferative activities

Table 2 Antiproliferative activities of title compounds (IC_{50}, μM)

Compd.	HUVEC	MCF-7	MV4-11
S21	11.67	10.49	0.12
S22	15.18	39.48	0.54
S23	12.64	28.79	0.34
S24	7.95	37.44	0.61
Linifanib	40.11	17.03	0.69

Because the four compounds **S21**–**S24** showed potent inhibitory activities against the three enzymes, so we selected these four compounds to evaluate their antiproliferative activity against human umbilical vein endothelial cells (HUVEC), human breast adenocarcinoma cell line (MCF-7) and human leukemia cell lines (MV4-11) through the CellTiter-Glo (CTG) cell growth inhibition test module.[24] HUVECs, derived from the endothelium of veins from the umbilical cord, are the most commonly studied human endothelial cell type in angiogenesis.[25] The ability of these derivatives to inhibit the cell growth was summarized in Table 2 with Linifanib as positive control. All the four compounds showed potent antiproliferative activity against HUVEC with their IC_{50} values were 11.67 μM, 15.18 μM, 12.64 μM and 7.95 μM respectively, and the IC_{50} value of Linifanib against HUVEC was only 40.11 μM. They also showed more potent inhibitory activities than Linifanib against MV4-11 with their IC_{50} values were 0.12 μM, 0.54 μM, 0.34 μM and 0.61 μM respectively. For the MCF-7, only **S21** was more potent than Linifanib with its IC_{50} value of 10.49 μM.

2.2.3. Docking studies

Because compound **S21** was very potent to inhibit the three kinases with its IC_{50}s against FLT3, KDR and PDGFR-β were 4 nM, 3 nM and 8 nM respectively, and S21 also showed potent antiproliferative activities against HUVEC, MCF-7 and MV4-11. So in order to further investigate the action mechanism of the **S21**, we performed molecular docking studies to investigate the binding modes and rationalize the efficiency. Compound **S21** was docked into the ATP-bind site of FLT3 (PDB ID: 4RT7), KDR (PDB ID: 1YWN) and PDGFR-β (PDB ID: 3MJG) which were obtained from the Protein Data Bank (RCSB PDB).[26] The binding mode of **S21** into the active site of three RTKs was shown in Figure 4.

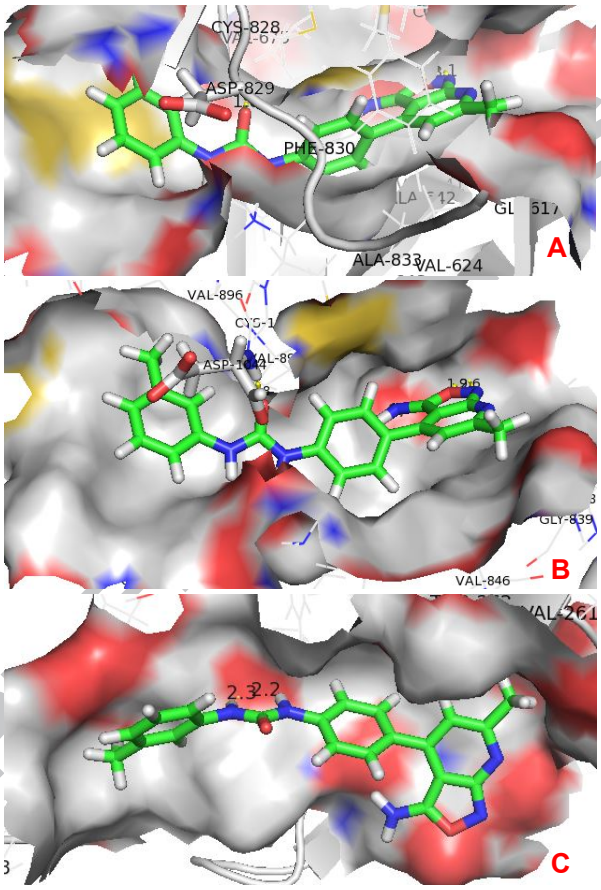

Figure 4. Interaction between compound **S21** and FLT3 (PDB ID: 4RT7) (**A**), KDR (PDB ID: 1YWN) (**B**) and PDGFR-β (PDB ID: 3MJG) (**C**). Hydrogen bonds are shown as yellow lines.

Compound **S21** bound across the hydrophobic pocket and ATP binding site of FLT3 through five hydrogen bonds (Fig. 4A). The nitrogen atom and oxygen atom in isoxazole ring formed two hydrogen bonds with Cys 694 with the length were 2.1 Å and 1.8 Å respectively. The amino group formed a hydrogen bond to Glu 692 with length of 1.9 Å. The carbonyl group in urea moity formed one hydrogen bond with Asp 829 with the length of 1.8 Å, and one NH of the urea moiety formed one hydrogen bond with Glu 661 with distance of 1.7 Å. For complex of compound **S21** with KDR (Fig. 4B), there were also five hydrogen bonds consisting the binding. The nitrogen atom and oxygen atom in isoxazole ring formed two hydrogen bonds with Cys 917 with the length were 2.6 Å and 1.9 Å respectively. The carbonyl group in urea moity formed one hydrogen bond with the length of 1.8 Å, and two NH of the urea moiety formed two hydrogen bonds with Glu

883 with distances were both 1.9 Å. For complex of compound **S21** with PDGFR-β (Fig. 4C), only the two NH of the urea moiety formed two hydrogen bonds with Glu 241. This information confirmed that the urea moiety was very important to form hydrogen bonds with various RTKs. Furthermore, the isoxazole could serve as a favorable pharmacophore, it played an essential role in binding with the ATP-bind site of FLT3 and KDR.

3. Conclusion

In this study, we designed and synthesized diaryl-ureas with novel isoxazol[3,4-*b*]pyridine-3-amino-structure using Linifanib as a lead compound, considering that the multi-target inhibitors against RTKs are highly useful anticancer agents with improved clinical efficacies. The kinase inhibitory and anticancer activities showed that some diaryl-ureas exhibited comparable potency with Linifanib. Fortunately, compound **S21** was identified as the most potent inhibitor against FLT3, KDR and PDGFR-β with its IC_{50} values were 4 nM, 3 nM and 8 nM respectively, it also showed potent inhibitory activities against several caner cells, docking studies showed that the urea moiety and isoxazole ring could form hydrogen bonds with the ATP-bind sites in RTKs. **S21** could be used as novel lead compound to further develop multi-target inhibitors against RTKs.

4. Experimental

4.1. Chemical synthesis

Reagents and solvents were purchased from commercial sources and used without further purification unless otherwise specified. Air- and moisture-sensitive liquids and solutions were transferred via syringe or stainless steel cannula. Organic solutions were concentrated by rotary evaporation below 45 °C at approximately 20 mmHg. All non-aqueous reactions were carried out under anhydrous conditions using flame-dried glassware in a nitrogen atmosphere in dry, freshly distilled solvents, unless otherwise noted. Yields refer to chromatographically and spectroscopically (^{1}H NMR) homogeneous materials, unless otherwise stated. Reactions were monitored by thin-layer chromatography (TLC) carried out on 0.15–0.20 mm Yantai silica gel plates (RSGF 254) using UV light as the visualizing agent. Chromatography was performed on Qingdao silica gel (160–200 mesh) with petroleum ether (60–90) and ethyl acetate mixtures as eluant. Melting points (Mp) were measured on a WRS-1B apparatus and were uncorrected. ^{1}H NMR spectra were obtained with a Bruker AV-300 (300 MHz). Chemical shifts are recorded in ppm downfield from tetramethylsilane. *J* values are given in Hz. Abbreviations used are s (singlet), d (doublet), t (triplet), q (quartet), b (broad) and m (multiplet). ESI-MS spectra were recorded on a Waters Synapt HDMS spectrometer.

4.1.1 The synthesis of S11–S110

*(E)-3-(4-Nitrophenyl)-1-phenylprop-2-en-1-one (**3**)*

A mixture of acetophenone (**1**) (6 g, 0.05 mol) and 4-nitro-benzaldehyde (**2**) (7.5 g, 0.05 mol) was stirred in EtOH (120 mL) at 0–5 °C, then 100 mL solution of NaOH (1 N) in water was added dropwise into the reaction mixture under stirring. After the mixture was allowed to stir for 24 h at 25°C, the ph value of the solution was adjusted to 7 by dilute hydrochloric acid (1 N), the yellow solid obtained was collected by filtration, washed with water, and dried under vacuum to produce **3** (10.88 g, 86%) as a yellow solid. Mp 167–169 °C.[16] ^{1}H NMR (300 MHz, DMSO-d_6) δ 8.21 (d, *J* = 8.8 Hz, 2H), 8.11 (d, *J* = 15.8 Hz, 1H), 7.93 (d, *J* = 15.8 Hz, 1H), 7.72 (d, *J* = 8.8 Hz, 2H), 7.62-7.66 (m, 2H), 7.47-7.53 (m, 3H). ESI-MS *m/z*: 252 $[M-H]^-$, 254 $[M+H]^-$, 276 $[M+Na]^-$.

*2-(1-(4-Nitrophenyl)-3-oxo-3-phenylpropyl)malononitrile (**4**)*

Bu_3P (280 μl, 0.001 mmol) was added to a solution of **3** (8 g, 0.032 mol) and malononitrile (6.6 g, 0.1 mol) in anhydrous CH_2Cl_2 (25 mL), after the mixture was refluxed under N_2 at room temperature for 2h, the white solid appeared was obtained by filtration to produce **4** (7.96 g, 78%). Mp 150–152 °C.[17] ^{1}H NMR (300 MHz, DMSO-d_6) δ 8.21 (d, J = 8.5 Hz, 2H), 8.01 (d, J = 7.5Hz, 2H), 7.8 (d, J = 8.5Hz, 2H), 7.59-7.62 (m, 1H), 7.51-7.54 (m, 2H), 5.32 (d, J = 10.4 Hz, 1H), 4.01 (d, J =10.4 Hz, 2H), 5.29-5.32 (m, 1H). ESI-MS *m/z*: 318 $[M-H]^-$, 320 $[M+H]^+$, 342 $[M+Na]^+$.

*4-(4-Nitrophenyl)-6-phenylisoxazolo[3,4-b]pyridin-3-amine (**5**)*

A solution of KOH (0.42 g, 7.5 mmol) in MeOH (60 ml) was added dropwise into the reaction mixture of **4** (0.77 g, 2.4 mmol) and hydroxylamine hydrochloride (0.33 g, 4.8 mmol) in MeOH (40 ml) in 1 h at 0–5 °C, then the reaction mixture was warmed to 25 °C and stirred for 24 h, the solid appeared was filtered to afford **5** (0.61 g, 77%) as a yellow solid. Mp > 300 °C.[18] ^{1}H NMR (300 MHz, DMSO-d_6) δ 8.38 (d, J = 8.7 Hz, 2H), 8.20-8.24 (m, 2H), 8.03 (d, J = 8.7Hz, 2H), 7.89 (s, 1H), 7.47-7.51 (m, 3H), 5.62 (s, 2H). ESI-MS *m/z*: 331 $[M-H]^-$, 333 $[M+H]^+$, 355 $[M+Na]^+$.

*4-(4-Aminophenyl)-6-phenylisoxazolo[3,4-b]pyridin-3-amine (**6**)*

Stannous chloride dehydrate (1.2 g 0.53 mmol) was added to a solution of compound **5** (0.8 g, 2.4 mmol) dissolved in 95% ethanol (50 ml), after the mixture was refluxed under N_2 for 3 h, the reaction mixture was partitioned between 200 ml dichloromethane and 200 ml water. The dichloromethane layer was washed with brine, dried over $MgSO_4$, filtered and concentrated. The crude material was purified by column chromatography (2% methanol in dichloromethane) to yield **6** (645 mg, 89%) as a yellow solid. Mp 229–231 °C. ^{1}H NMR (300 MHz, DMSO-d_6) δ 8.19 (d, J = 8.4 Hz, 2H), 7.72 (s, 1H), 7.47-7.53 (m, 5H), 6.73 (d, J = 8.4 Hz, 2H), 5.7 (s, 2H), 5.5 (s, 2H). ESI-MS *m/z*: 301 $[M-H]^-$, 303 $[M+H]^+$, 325 $[M+Na]^+$.

The substituted isocyanates (0.6~0.8mmol) was added into a solution of compound **6** (60 mg, 0.2 mmol) dissolved in anhydrous EtOH (13 mL) at 25 °C, followed by catalytic amount of triethylamine, after stirring at 25 °C for 2 h, the solid obtained was purified by column chromatography on silica gel using 30% ethyl acetate in petroleum ether as eluent to afford **S11–S10** as yellow solids.

*1-(4-(3-Amino-6-phenylisoxazolo[3,4-b]pyridin-4-yl)phenyl)-3-m-tolylurea (**S11**)*

Synthesized from **14a**. Yield 76%. Mp 228–230 °C. ^{1}H-NMR (300 MHz, DMSO-d_6) δ 9.00 (s, 1H), 8.73 (s, 1H), 8.25 (d, J = 8.7 Hz, 2H), 7.86 (s, 1H), 7.68-7.71 (m, 4H), 7.53-7.57 (m, 3H), 7.34 (s, 1H), 7.26-7.29 (m, 1H), 7.16-7.18 (m, 1H), 6.82 (d, J = 7.41 Hz, 1H), 5.60 (s, 2H), 2.30 (s, 3H). ESI-MS *m/z*: 434 $[M-H]^-$, $[M+H]^+$ 436, $[M+Na]^+$ 458.

*1-(4-(3-Amino-6-phenylisoxazolo[3,4-b]pyridin-4-yl)phenyl)-3-(4-fluorophenyl)urea (**S12**)*

Synthesized from **14b**. Yield 73%. Mp 229–231 °C. ^{1}H-NMR (300 MHz, DMSO-d_6) δ 9.01 (s, 1H), 8.79 (s, 1H), 8.23 (m, 2H), 7.85 (s, 1H), 7.68-7.71 (m, 4H), 7.48-7.55 (m, 5H), 7.12-7.18 (m, 2H), 5.58 (s, 2H). ESI-MS *m/z*: 438 $[M-H]^-$, 440 $[M+H]^+$, 462 $[M+Na]^+$.

*1-(4-(3-Amino-6-phenylisoxazolo[3,4-b]pyridin-4-yl)phenyl)-3-phenylurea (**S13**)*

Synthesized from **14c**. Yield 79%. Mp 198–200 °C. ^{1}H-NMR (300 MHz, DMSO-d_6) δ 9.01 (s, 1H), 8.79 (s, 1H), 8.23-8.26 (m, 2H), 7.85 (s, 1H), 7.71-7.74 (m, 4H), 7.48-7.55 (m, 5H), 7.28-7.34 (t, 2H), 6.97-7.03 (t, 1H), 5.58 (s, 2H). ESI-MS *m/z*: 420 $[M-H]^-$, 422 $[M+H]^+$, 444 $[M+Na]^+$.

*1-(4-(3-Amino-6-phenylisoxazolo[3,4-b]pyridin-4-yl)phenyl)-3-(3-chlorophenyl)urea (**S14**)*

Synthesized from **14d**. Yield 85%. Mp 240–242 °C. ^{1}H-NMR (300 MHz, DMSO-d_6) δ 9.10 (s, 1H), 9.02 (s, 1H), 8.19-8.21 (m, 2H), 7.80 (s, 1H), 7.68-7.72 (m, 5H), 7.49-7.53 (m, 3H), 7.31-

7.34 (m, 2H), 7.01-7.04 (m, 1H), 5.5 (s, 2H). ESI-MS *m/z*: 454 $[M-H]^-$, 456 $[M+H]^+$, 478 $[M+Na]^+$.

*1-(4-(3-Amino-6-phenylisoxazolo[3,4-b]pyridin-4-yl)phenyl)-3-p-tolylurea (**S15**)*

Synthesized from **14e**. Yield 84%. Mp 244–245 °C. ^{1}H-NMR (300 MHz, DMSO-d_6) δ 8.97 (s, 1H), 8.69 (s, 1H), 8.23-8.26 (m, 2H), 7.85 (s, 1H), 7.68-7.72 (m, 4H), 7.50-7.58 (m, 3H), 7.36-7.39 (m, 2H), 7.10-7.13 (m, 2H), 5.60 (s, 2H), 2.26 (s, 3H). ESI-MS *m/z*: 434 $[M-H]^-$, 436 $[M+H]^+$, 458 $[M+Na]^+$.

*1-(4-(3-Amino-6-phenylisoxazolo[3,4-b]pyridin-4-yl)phenyl)-3-(4-methoxyphenyl)urea (**S16**)*

Synthesized from **14f**. Yield 88%. Mp 189–190 °C. ^{1}H-NMR (300 MHz, DMSO-d_6) δ 8.99 (s, 1H), 8.62 (s, 1H), 8.24-8.26 (m, 2H), 7.85 (s, 1H), 7.73-7.77 (m, 4H), 7.53-7.57 (m, 3H), 7.29-7.33 (m, 2H), 6.84-6.91 (m, 2H), 5.60 (s, 2H), 3.71 (s, 3H). ESI-MS *m/z*: 450 $[M-H]^-$, 452 $[M+H]^+$, 474 $[M+Na]^+$.

*1-(4-(3-Amino-6-phenylisoxazolo[3,4-b]pyridin-4-yl)phenyl)-3-(4-chloro-3-(trifluoromethyl)phenyl)urea (**S17**)*

Synthesized from **14g**. Yield 74%. Mp 263–265 °C. ^{1}H-NMR (300 MHz, DMSO-d_6) δ 9.30 (s, 1H), 9.20 (s, 1H), 8.23-8.26 (m, 2H), 8.15 (d, J = 2.01 Hz, 1H), 7.86 (s, 1H), 7.71-7.75 (m, 4H), 7.66-7.68 (m, 2H), 7.53-7.56 (m, 3H), 5.59 (s, 2H). ESI-MS *m/z*: 522 $[M-H]^-$, 524 $[M+H]^+$, 546 $[M+Na]^+$.

*1-(4-(3-Amino-6-phenylisoxazolo[3,4-b]pyridin-4-yl)phenyl)-3-(3-fluorophenyl)urea (**S18**)*

Synthesized from **14h**. Yield 83%. Mp 237–239 °C. ^{1}H-NMR(300 MHz, DMSO-d_6) δ 9.17 (s, 1H), 9.12 (s, 1H), 8.23-8.26 (m, 2H), 7.86 (s, 1H), 7.71-7.74 (m, 4H), 7.52-7.56 (m, 4H), 7.30-7.37 (m, 1H), 7.12-7.23 (m, 1H), 6.75-6.85 (m, 1H), 5.60 (s, 2H). ESI-MS *m/z*: 438 $[M-H]^-$, 440 $[M+H]^+$, 462 $[M+Na]^+$.

*1-(4-(3-Amino-6-phenylisoxazolo[3,4-b]pyridin-4-yl)phenyl)-3-(2-fluorophenyl)urea (**S19**)*

Synthesized from **14i**. Yield 81%. Mp 238–240 °C. ^{1}H-NMR (300 MHz, DMSO-d_6) δ 9.40 (s, 1H), 8.68 (s, 1H), 8.19-8.26 (m, 3H), 7.86 (s, 1H), 7.68-7.72 (m, 4H), 7.51-7.54 (m, 3H), 7.20-7.23 (m, 2H), 7.08 (s, 1H), 5.61 (s, 2H). ESI-MS *m/z*: 438 $[M-H]^-$, 440 $[M+H]^+$, 462 $[M+Na]^+$.

*1-(4-Acrylamidophenyl)-3-(4-(3-amino-6-phenylisoxazolo[3,4-b]pyridin-4-yl)phenyl)urea (**S110**)*

Synthesized from **18a**. Yield 82%. Mp > 300 °C. ^{1}H-NMR (300 MHz, DMSO-d_6) δ 10.10 (s, 1H), 9.05 (s, 1H), 8.81 (s, 1H), 8.24-8.26 (m, 2H), 7.86 (s, 1H), 7.65-7.70 (m, 2H, 7.43-7.63(m, 9H), 6.40-6.48 (m, 1H), 6.21-6.26 (m, 1H), 5.72-5.76 (m, 1H), 5.53 (s, 2H). ESI-MS *m/z*: 489 $[M-H]^-$, 491 $[M+H]^+$, 513 $[M+Na]^+$.

4.1.2 The synthesis of S21–S28

*(E)-4-(4-Nitrophenyl)but-3-en-2-one (**8**)*

K_2CO_3 in water (0.02 mol, 20 ml) was added into a solution of *p*-nitrobenzaldehyde (15 g, 0.1 mol) in acetone (250 ml), after the mixture stirred at 25 °C for 24 h, concentrated hydrochloric acid (40 ml) was added into the solution and the reaction was stirred for another 8 h, at last, 200 ml water was added and the solid appeared was collected by filtration and purified by column chromatography (20% ethyl acetate in petroleum ether) to yield **8** (16.2 g, 85%) as a yellow solid. Mp 250–252°C.[17] ^{1}H NMR (300 MHz, DMSO-d_6) δ 8.24 (d, J = 8.8 Hz, 2H), 7.69 (d, J = 8.8 Hz, 2H), 7.51 (d, J = 15.8 Hz, 1H), 6.84 (d, J = 15.8 Hz, 1H), 2.41 (s, 3H). ESI-MS *m/z*: 190 $[M-H]^-$, 192 $[M+H]^+$, 214 $[M+Na]^+$.

*6-Methyl-4-(4-nitrophenyl)-2-oxo-1,2-dihydropyridine-3-carbonitrile (**9**)*

t-BuOK (4 g, 35.6 mmol) was added into a solution of **8** (4 g, 20.9 mmol) and

cyanoacetamide (3.3 g, 39.2 mmol) in DMSO (40 ml), after the mixture stirred at 25 °C for 1h, *t*-BuOK (8g, 71.2mmol) was added and the mixture stirred for another 2h, then 200 ml water was added and dilute hydrochloric acid solution (4 N, 150 ml) was added to adjust the pH to be 2, the solid appeared was obtained by filtration and dried under vacuum to afford **9** (4.4 g, 83%). Mp 183–185 °C.[19] ^{1}H NMR (300 MHz, DMSO-d_6) δ 8.72 (s, 1H), 8.26 (d, J = 8.8 Hz, 2H), 7.63 (d, J = 8.8 Hz, 2H), 5.58 (s, 1H), 1.84 (s, 3H). ESI-MS *m/z*: 254 $[M-H]^-$, 256 $[M+H]^+$, 278 $[M+Na]^+$.

*2-Chloro-6-methyl-4-(4-nitrophenyl)nicotinonitrile (**10**)*

9 (6.2 g, 24.3 mmol) was added into a solution of $POCl_3$ (40 ml), after the reaction mixture was refluxed for 2 h, 500 ml ice water was added, the solid obtained by filtration was purified by column chromatography (20% ethyl acetate in petroleum ether) to yield **10** (5.1 g, 77%) as a yellow solid. Mp 168–170 °C. ^{1}H-NMR (300 MHz, DMSO-d_6) δ 8.39 (d, J = 8.7Hz, 2H), 7.82 (d, J = 8.7Hz, 2H), 7.31 (s, 1H), 2.53 (s, 3H). ESI-MS *m/z*: 272 $[M-H]^-$, $[M+H]^+$ 274, 296 $[M+Na]^+$.

*4-(4-Aminophenyl)-2-chloro-6-methylnicotinonitrile (**11**)*

The iron powder (1.51 g, 27 mmol) and glacial acetic acid (3 ml) were added into a solution of **10** (1.91 g, 7 mmol) in ethanol (120 ml), after the mixture was refluxed for 2 h, the reaction mixture was partitioned between 100 ml EtOAc and 50×4 ml water. The EtOAc layer was washed with brine, dried over $MgSO_4$, filtered, concentrated and purified by by column chromatography on silica gel using 25% ethyl acetate in petroleum ether as eluent to afford **11** (1.51g, 89%) as a yellow solid. Mp 122–124 °C. ^{1}H-NMR (300 MHz, DMSO-d_6) δ 7.49 (s, 1H), 7.41 (d, J = 8.5Hz, 2H), 6.7 (d, J = 8.5Hz, 2H), 5.8 (s, 2H), 2.5 (s, 3H). ESI-MS *m/z*: 242 $[M-H]^-$, 244 $[M+H]^+$, 266 $[M+Na]^+$.

*4-(4-Aminophenyl)-6-methylisoxazolo[3,4-b]pyridin-3-amine (**12**)*

Hydroxylamine hydrochloride (530 mg, 7.6 mmol) was added into a solution of **11** (340 mg, 1.4 mmol) in *t*-BuOH (50 ml), after the mixture was refluxed for 2 h, *t*-BuOK (896 mg, 8 mmol) was added and the mixture was refluxed for another 0.5 h, 200 ml methanol was added and the mixture was filtrated, dried over anhydrous Na_2SO_4, filtered and concentrated. The crude material was purified by column chromatography (2% methanol in dichloromethane) to yield **12** (232 mg, 69%) as a yellow solid. Mp 205–207 °C. ^{1}H-NMR (300 MHz, DMSO-d_6) δ 7.39 (d, J = 8.4Hz, 2H), 7.01 (s, 1H), 6.72 (d, J = 8.4Hz, 2H), 5.81 (s, 2H), 5.38 (s, 2H), 2.52 (s, 3H). ESI-MS *m/z*: 239 $[M-H]^-$, $[M+H]^+$ 241, 263 $[M+Na]^+$.

The substituted isocyanate (0.9~1.2 mmol) was added into a solution of compound **12** (72 mg, 0.3 mmol) dissolved in anhydrous EtOH (15 mL) at 25 °C, followed by catalytic amount of triethylamine, after stirring at 25 °C for 2 h, the solid obtained was purified by column chromatography on silica gel using 2% MeOH in CH_2Cl_2 as eluent to afford **S21–S28** as yellow solids.

*1-(4-(3-Amino-6-methylisoxazolo[3,4-b]pyridin-4-yl)phenyl)-3-m-tolylurea (**S21**)*

Synthesized from **14a**. Yield 67%. Mp 144–146 °C. ^{1}H-NMR (300 MHz, DMSO-d_6) δ 8.96 (s, 1H), 8.71 (s, 1H), 7.67 (d, J = 8.56, 2H), 7.56 (d, J = 8.56, 2H), 7.33 (s, 1H), 7.25-7.28 (m, 1H), 7.12-7.19 (m, 2H), 6.81 (d, J = 7.41, 1H), 5.60 (s, 2H), 2.59 (s, 3H), 2.29 (s, 3H). ESI-MS: m/z 372 $[M-H]^-$, 374 $[M+H]^+$, 396 $[M+Na]^+$.

*1-(4-(3-Amino-6-methylisoxazolo[3,4-b]pyridin-4-yl)phenyl)-3-(3-chlorophenyl)urea (**S22**)*

Synthesized from **14d**. Yield 81%. Mp 165–167 °C. ^{1}H-NMR(300 MHz, DMSO-d_6) δ 9.09 (s,

1H), 9.03 (s, 1H), 7.74 (s, 1H), 7.68 (d, *J* = 8.6 Hz, 2H), 7.57 (d, *J* = 8.6 Hz, 2H), 7.28-7.36 (m, 2H), 7.20 (s, 1H), 7.03-7.06 (m, 1H), 5.50 (s, 2H), 2.51 (s, 3H). ESI-MS *m/z*: 392 $[M-H]^-$, $[M+H]^+$ 394, $[M+Na]^+$ 416.

1-(4-(3-Amino-6-methylisoxazolo[3,4-b]pyridin-4-yl)phenyl)-3-(4-chloro-3-(trifluoromethyl)phenyl)urea ***(S23)***

Synthesized from **14g**. Yield 69%. Mp 150–151 °C. ^{1}H-NMR (300 MHz, DMSO-d_6) δ 9.30 (s, 1H), 9.18 (s, 1H), 8.15 (s, 1H), 7.67-7.76 (m, 4H), 7.57-7.62 (m, 2H), 7.20 (s, 1H), 5.52 (s, 2H), 2.60 (s, 3H). ESI-MS *m/z*: 460 $[M-H]^-$, 462 $[M+H]^+$, 484 $[M+Na]^+$.

1-(4-(3-Amino-6-methylisoxazolo[3,4-b]pyridin-4-yl)phenyl)-3-(3-(trifluoromethyl)phenyl)urea ***(S24)***

Synthesized from **14k**. Yield 65%. Mp 135–137 °C. ^{1}H-NMR (300 MHz, DMSO-d_6) δ 9.19 (s, 1H), 9.13 (s, 1H), 8.05 (s, 1H), 7.59-7.67(m, 2H), 7.51-7.56 (m, 4H), 7.33-7.35 (m, 1H), 7.19 (s, 1H), 5.50 (s, 2H), 2.67 (s, 3H). ESI-MS *m/z*: 426 $[M-H]^-$, 428 $[M+H]^+$, 450 $[M+Na]^+$.

1-(4-(3-Amino-6-methylisoxazolo[3,4-b]pyridin-4-yl)phenyl)-3-(2-chlorophenyl)urea ***(S25)***

Synthesized from **14l**. Yield 82%. Mp 238–240 °C. ^{1}H-NMR (300 MHz, DMSO-d_6) δ 9.71 (s, 1H), 8.43 (s, 1H), 8.18 (d, *J* = 7.53Hz, 1H), 7.67-7.70 (m, 2H), 7.57-7.60 (m, 2H), 7.47-7.50 (m, 1H), 7.30-7.35 (t, *J* = 7.5 Hz, 1H), 7.20 (s, 1H), 7.04-7.09 (t, *J* = 7.05Hz, 1H), 5.51 (s, 2H), 2.60 (s, 3H). ESI-MS *m/z*: 392 $[M-H]^-$, 394 $[M+H]^+$, 416 $[M+Na]^+$.

(Z)-1-(4-(3-Amino-6-methylisoxazolo[3,4-b]pyridin-4-yl)phenyl)-3-(4-but-2-enamidophenyl)urea ***(S26)***

Synthesized from **18b**. Yield 66%. Mp 281–283 °C. ^{1}H-NMR (300 MHz, DMSO-d_6) δ 9.89 (s, 1H), 8.97 (s, 1H), 8.75 (s, 1H), 7.65-7.68 (m, 2H), 7.54-7.59 (m, 4H), 7.40-7.46 (m, 2H), 7.19 (s, 1H), 6.73-6.83 (m, 1H), 6.08-6.14 (dd, J_1 = 1.4 Hz, J_2 = 15.1 Hz, 1H), 5.50 (s, 2H), 2.60 (s, 3H), 1.86 (d, *J* = 5.9 Hz, 3H). ESI-MS *m/z*: 441 $[M-H]^-$, 443 $[M+H]^+$, 465 $[M+Na]^+$.

(Z)-1-(4-(3-Amino-6-methylisoxazolo[3,4-b]pyridin-4-yl)phenyl)-3-(4-but-2-enamido-3-methylphenyl)urea ***(S27)***

Synthesized from **18c**. Yield 79%. Mp 266–268 °C. ^{1}H-NMR (300 MHz, DMSO-d_6) δ 9.44 (s, 1H), 9.24 (s, 1H), 9.14 (s, 1H), 7.67 (d, *J* = 8.6 Hz, 2H), 7.55 (d, *J* = 8.6 Hz, 2H), 7.25-7.34 (m, 3H), 7.20 (s, 1H), 6.75 (dd, J_1 = 6.9 Hz, J_2 = 15.2 Hz, 1H), 6.20 (d, *J* = 14.6 Hz, 1H), 5.48 (s, 2H), 2.59 (s, 3H), 2.17 (s, 3H), 1.86 (d, *J* = 6.5 Hz, 3H). ESI-MS *m/z*: 455 $[M-H]^-$, 457 $[M+H]^+$, 479 $[M+Na]^+$.

1-(4-(3-Amino-6-methylisoxazolo[3,4-b]pyridin-4-yl)phenyl)-3-(3-methyl-4-(2-(morpholinomethyl)acrylamido)phenyl)urea ***(S28)***

Synthesized from **25**. Yield 76%. Mp 144–146 °C. ^{1}H-NMR (300 MHz, DMSO-d_6) δ 10.39 (s, 1H), 10.24 (s, 1H), 10.01 (s, 1H), 7.83 (d, *J* = 8.7 Hz, 1H), 7.69 (d, *J* = 8.6 Hz, 2H), 7.54 (d, *J* = 8.6 Hz, 2H), 7.38 (s, 1H), 7.30-7.34 (m, 1H), 7.20 (s, 1H), 6.7(m, 1H), 6.14 (d, *J* = 1.5 Hz, 1H), 5.61 (d, *J* = 1.5 Hz, 1H), 5.50 (s, 2H), 4.17-4.22 (t, 2H), 3.64-3.67 (t, 4H), 3.15-3.18 (t, 4H), 2.59 (s, 3H), 2.29 (s, 3H). ESI-MS *m/z*: 540 $[M-H]^-$, 542 $[M+H]^+$, 564 $[M+Na]^+$.

4.1.3 The synthesis of side chains

The synthesis of isocyanates ***14a–14l***

A solution of substituted aniline (0.01 mol) in ethyl acetate (20 ml) was added dropwise to a solution of triphosgene (1.5 g, 0.005 mol) dissolved in ethyl acetate (20 ml) at 0 °C, after the mixture reacted at 0 °C for 0.5 h, then it was warmed to room temperature and reacted for 1 h. At

last, the mixture refluxed for another 4–6 h. The solvent was distilled at reduced pressure to afford the side chain **14a~14l** which could be used directly for the next reaction without further purification.[20,21]

*The synthesis of isocyanate **18a–18c***

Substituted acryloyl chloride (29 mmol) and DIPEA (5 ml, 29 mmol) were added into a solution of substituted aniline (**15**) (13 mmol) in EtOAc (100 ml), after the mixture was stirred at 25°C for 3h, the reaction mixture was partitioned between 100 ml EtOAc and 200 ml water. The EtOAc layer was washed with brine, dried over $MgSO_4$, filtered and concentrated to yield **16** as yellow solids.[22,23]

16a, yield 88%. ^{1}H-NMR (300 MHz, DMSO-d_6) δ 8.18 (d, J = 9.2 Hz, 2H), 7.93 (s, 1H), 7.70 (d, J = 9.2 Hz, 2H), 6.43-6.51 (m, 1H), 6.18-6.23 (m, 1H), 5.74-5.78 (m, 1H). ESI-MS *m/z*: 191 $[M-H]^-$, 193 $[M+H]^+$, 215 $[M+Na]^+$.

16b, yield 85%. ^{1}H-NMR (300 MHz, DMSO-d_6) δ 8.20 (d, J = 9.1 Hz, 2H), 7.91 (s, 1H), 7.68 (d, J = 9.1 Hz, 2H), 5.78-5.83 (m, 1H), 5.58 (d, J = 15.1 Hz, 1H), 2.01 (d, J = 6.4 Hz, 3H). ESI-MS *m/z*: 205 $[M-H]^-$, 207 $[M+H]^+$, 229 $[M+Na]^+$.

16c, yield 93%. ^{1}H-NMR (300 MHz, DMSO-d_6) δ 8.41 (d, J = 8.5 Hz, 1H), 8.11-8.14 (m, 2H), 7.28 (s, 1H), 7.00-7.04 (m, 1H), 6.02 (d, J = 15.1 Hz, 1H), 2.38 (s, 3H), 2.01 (d, J = 6.4 Hz, 3H). ESI-MS *m/z*: 219 $[M-H]^-$, 221 $[M+H]^+$, 243 $[M+Na]^+$.

The iron powder (1.52 g, 27 mmol) and glacial acetic acid (3 ml) were added into a solution of **16** (7 mmol) in ethanol (120 ml), after the mixture was refluxed for 2 h, the reaction mixture was partitioned between 100 ml EtOAc and 50×4 ml water. The EtOAc layer was washed with brine, dried over $MgSO_4$, filtered, concentrated and purified by by column chromatography on silica gel using 25% ethyl acetate in petroleum ether as eluent to afford **17** as yellow oil.[27,28]

17a, yield 91%. ^{1}H-NMR (300 MHz, DMSO-d_6) δ 9.65 (s, 1H), 7.31 (d, J = 8.8 Hz, 2H), 6.53 (d, J = 8.8 Hz, 2H), 6.28-6.32 (m, 1H), 6.15-6.19 (m, 1H), 5.66-5.71 (m, 1H), 4.85 (s, 2H). ESI-MS *m/z*: 161 $[M-H]^-$, 163 $[M+H]^+$, 185 $[M+Na]^+$.

17b, yield 82%. ^{1}H-NMR (300 MHz, DMSO-d_6) δ 9.71 (s, 1H), 7.28 (d, J = 8.7 Hz, 2H), 6.56 (d, J = 8.7 Hz, 2H), 5.69-5.73 (m, 1H), 5.42 (d, J = 14.8 Hz, 1H), 4.91 (s, 2H), 2.01 (d, J = 6.2 Hz, 3H). ESI-MS *m/z*: 175 $[M-H]^-$, 177 $[M+H]^+$, 199 $[M+Na]^+$.

17c, yield 88%. ^{1}H-NMR (300 MHz, DMSO-d_6) δ 7.31 (s, 1H), 6.98-7.03 (m, 3H), 6.47-6.52 (m, 1H), 5.88 (d, J = 15.1 Hz, 1H), 3.6 (s, 2H), 2.22 (s, 3H), 1.91 (d, J = 5.9 Hz, 3H). ESI-MS *m/z*: 189 $[M-H]^-$, 191 $[M+H]^+$, 213 $[M+Na]^+$.

Triphosgene (1.5 g, 0.005 mol) in ethyl acetate (20 ml) was added dropwise to a solution of **17** (0.01 mol) in ethyl acetate (20 ml) at 0 °C, after the mixture reacted at 0 °C for 0.5 h, then it was warmed to room temperature and reacted for 1h. At last, the mixture refluxed for another 4–6 h. The solvent was distilled at reduced pressure to afford the side chain **18a–18c** which could be used directly for the next reaction without further purification.

*The synthesis of isocyanate **25***

Acryloyl chloride (2.4 ml, 29 mmol) and DIPEA (5 ml, 29 mmol) were added into a solution of 2-methyl-4-nitroaniline (**19**) (2 g, 13 mmol) in EtOAc (100 ml), after the mixture was stirred at 25 °C for 3 h, the reaction mixture was partitioned between 100 ml EtOAc and 200 ml water. The EtOAc layer was washed with brine, dried over $MgSO_4$, filtered and concentrated to yield **20** (2.28 g, 85%) as a yellow solid. ^{1}H-NMR (300 MHz, DMSO-d_6) δ 9.27 (s, 1H), 7.80 (s, 1H), 7.72-7.76 (m, 1H), 7.58-7.62 (m, 1H), 6.41-6.48 (m, 1H), 6.20-6.24 (m, 1H), 5.71-5.75 (m, 1H), 2.52 (s, 3H).

ESI-MS *m/z*: 205 $[M-H]^-$, 207 $[M+H]^+$, 229 $[M+Na]^+$.

DABCO (1 g, 9 mmol) and paraformaldehyde (0.45 g, 15 mmol) were added into a solution of **20** (0.62 g, 3 mmol) in 1,4-dioxane:H_2O (5:3), after the mixture was reacted for 8 h at 80 °C, the reaction mixture was partitioned between 100 ml EtOAc and 200 ml water. The EtOAc layer was washed with brine, dried over $MgSO_4$, filtered and concentrated to yield **21** (0.62 g, 88%) as a white solid. ^{1}H-NMR (300 MHz, DMSO-d_6) δ 9.22 (s, 1H), 7.84 (s, 1H), 7.76-7.80 (m, 1H), 7.62-7.66 (m, 1H), 6.73 (s, 1H), 6.37 (s, 1H), 4.12 (s, 2H), 3.32 (s, 1H), 2.54 (s, 3H). ESI-MS *m/z*: 235 $[M-H]^-$, 237 $[M+H]^+$, 259 $[M+Na]^+$.

PBr_3 (0.34 g, 1.2 mmol) was added into a solution of **21** (0.24 g, 1 mmol) in DCM (30 ml), after the mixture was reacted for 30 min at 25 °C, the reaction mixture was partitioned between 80 ml DCM and 50×3 ml water. The DCM layer was washed with brine, dried over $MgSO_4$, filtered and concentrated to yield **22** (0.25 g, 84%) as a white solid. ^{1}H-NMR (300 MHz, DMSO-d_6) δ 9.24 (s, 1H), 7.83 (s, 1H), 7.78-7.81 (m, 1H), 7.68-7.71 (m, 1H), 6.68 (s, 1H), 6.32 (s, 1H), 3.85 (s, 2H), 2.52 (s, 3H). ESI-MS *m/z*: 297 $[M-H]^-$, 299 $[M+H]^+$, 321 $[M+Na]^+$.

Morpholine (0.27 g, 2.5 mmol) was added into a solution of **22** (0.15 g, 0.5 mmol) in DCM (30 ml), after the mixture was reacted for 30 min at 25 °C, the reaction mixture was partitioned between 80 ml DCM and 50×3 ml water. The DCM layer was washed with brine, dried over $MgSO_4$, filtered and concentrated to yield **23** (0.13 g, 85%) as a white solid. ^{1}H-NMR (300 MHz, DMSO-d_6) δ 9.21 (s, 1H), 7.80 (s, 1H), 7.70-7.73 (m, 2H), 6.70 (s, 1H), 6.11 (s, 1H), 3.59-3.62 (m, 4H), 3.31 (s, 2H), 2.57-2.59 (m, 4H), 2.54 (s, 3H). ESI-MS *m/z*: $[M-H]^-$ 304, $[M+H]^+$ 306, $[M+Na]^+$ 328.

The iron powder (1.52 g, 27 mmol) and glacial acetic acid (3 ml) were added into a solution of **23** (2.1 g, 7 mmol) in ethanol (120 ml), after the mixture was refluxed for 2 h, the reaction mixture was partitioned between 100 ml EtOAc and 50×4 ml water. The EtOAc layer was washed with brine, dried over $MgSO_4$, filtered, concentrated and purified by by column chromatography on silica gel using 25% ethyl acetate in petroleum ether as eluent to afford **24** (1.79 g, 93%) as yellow solid. ^{1}H-NMR (300 MHz, DMSO-d_6) δ 10.12 (s, 1H), 7.81 (d, J = 8.6 Hz, 1H), 7.45 (s, 1H), 7.38-7.42 (m, 1H), 6.68 (s, 1H), 6.16 (s, 1H), 3.89 (s, 2H), 3.61-3.65 (t, 4H), 3.28 (s, 2H), 3.11-3.15 (t, 4H), 2.28 (s, 3H). ESI-MS *m/z*: $[M-H]^-$ 274, $[M+H]^+$ 276, $[M+Na]^+$ 298.

Triphosgene (1.5 g, 0.005 mol) in ethyl acetate (20 ml) was added dropwise to a solution of **24** (0.01 mol) in ethyl acetate (20 ml) at 0°C, after the mixture reacted at 0 °C for 0.5 h, then it was warmed to room temperature and reacted for 1h. At last, the mixture refluxed for another 4–6h. The solvent was distilled at reduced pressure to afford the **25** which could be used directly for the next reaction.

4.2 Biological evaluation

4.2.1 In vitro kinase FLT3, KDR and PDGFR-β assay

Inhibition ratio determination and IC_{50} testing at a single concentration (10 μM) were entrusted to Reaction Biology Corporation. Cisbio's HTRF KinEASE Kit was used to test the enzyme inhibitory activity. This method utilizes a unique substrate containing a single phosphorylation site recognized by a europium cryptate (Eu(K))-labeled antibody to phosphotyrosine. Based on homogeneous time-resolved fluorescence (HTRF), all KinEASE assays involve two steps: the enzymatic step and the detection step with HTRF reagents. In the kinase reaction step, 2 μL of kinase (FLT3, KDR and PDGFR-β) solution, 2 μL of biotin substrate, and 4 μL of compound (SEB-supplemented kinase buffer) were added to each well for incubation.

Then, 2 μL of ATP was added at room temperature (18−22 °C) to initiate the reaction, which was run for 1 h. In the second step, detection reagents including 5 μL of streptavidin-XL665 (SA-XL665) in EDTA and 5 μL tyrosine kinase antibody-Eu(K) in EDTA were added to each well and incubated for 1 h at room temperature. The Beckman Coulter platform HTRF detection module was used to detect the signal. The detection reagents catch the phosphorylated substrate and the resulting HTRF signal is proportional to the amount of phosphorylation.[29] GraphPad Prism 5.0 software was used to calculate the IC_{50} values for each compound (https://www.graphpad.com/scientific-software/prism/). Each test was repeated three times.

4.2.2 Antiproliferative assay

All cell activity tests were entrusted to Crown Bioscience Inc. The luciferase in the CTG reagent uses luciferin, ATP and oxygen as substrates to produce oxidized luciferin and release energy in the form of light. The amount of light produced is proportional to the total amount of ATP, which can reflect the total number of viable cells (HUVECs, MCF-7, and MV4-11). The anticell proliferation rate can be calculated by the fluorescence intensity. This method included several steps. The first step was cell planking, where the cells in the exponential growth phase were collected and the viable cells were counted with Vi-Cell XR cell counting instrument. According to the density in the cell culture medium, the cell suspension was adjusted and 90 μL of medium was added to each well of a 96-well cell culture plate. The final cell concentration was approximately 2000−4000 cells per well (the specific cell density was adjusted according to cell growth). The next step was compound dispensation, where the target compound was dissolved from 10 μM stock solutions in DMSO, and then these solutions were diluted 10-fold with the medium solution. A total of 10 μL of the 10-fold compound dilution was added per well to each cell line, leading to a final drug concentration of 10 μM and a final DMSO concentration of 0.1%. The plate was placed in an incubator containing 5% CO_2 at 37 °C for 72 h. Next was the plate detection step, where according to the manufacturer instructions, 50 μL of CTG solution that was previously thawed and equilibrated to room temperature was added to each well after 72 h of drug treatment. A microplate oscillator was used to mix the solution for 2 min. After a 10 min incubation at room temperature, the fluorescence signal value was measured by an Envision2104 plate reader. Each compound was submitted for a 10 concentrations test (from 1 nM to 100 μM). Data processing: inhibition ratio = $1 - V_{\text{sample}}/V_{\text{vehicle control}} \times 100\%$. V_{sample} is for drug treatment group while $V_{\text{vehicle control}}$ is for solvent control group. The GraphPad Prism 5.0 software was used to draw nonlinear regression model and S type dose survival rate curve, and then calculate IC_{50} values. Each test was repeated three times.

4.3 Molecular dock modeling[30]

The binding modes of compound **S21** were investigated using molecular docking modeling in the AutoDock 4.2 software. Before starting the docking process, the protein structure was subjected to optimization step in order to minimize the crystallographic induced bond clashes. The Kollman united atom charges and polar hydrogen was added to the receptor and the crystallographic waters were removed. PyMol was used to display the 3D structure of the compound **S21** complexed with crystal structures. Charges of the Gasteiger type were assigned to the new constructed structures in AutoDock. Non-polar hydrogen atoms were merged and rotatable bonds were defined. The grid maps of the protein were calculated using AutoGrid

module embedded in AutoDock software. The grid was set in a way to include not only the active site amino acids but also the considerable portions of the surrounding surface. Hence, a grid size of 60 60 60 Å points and 0.375 Å spacing were generated based on the binding position of the cognate ligand in the protein. Docking simulations were performed using the autodock module of the software. Every docking program was taken out in 250,000 times energy evaluation with 10 conformations kept and the most favorable pose of each compound was exhibited.

Acknowledgments

This work was supported by the National Natural Science Foundation of China (81302634 and 21302225), China Scholarship Council (No. 201407060046), Natural Science Foundation of Jiangsu Province (BK20151563 and BK20130662), Six Talents Project Funded by Jiangsu Province (2013-YY-010), Jiangsu Collaborative Innovation Center of Chinese Medicinal Resources Industrialization (ZDXMHT-1-13), Project Funded by the Priority Academic Program Development of Jiangsu Higher Education Institutions and Project Funded by the Flagship Major Development of Jiangsu Higher Education Institutions (PPZY2015A070).

References

1. Bosso, M.; Ständker, L.; Kirchhoff, F.; Münch. J. *Bioorg. Med. Chem.* **2018**, *26*, 2719.
2. Carmeliet, P.; Jain, R. K. *Nature* **2000**, *407*, 249.
3. Zhang, H.; Wang, J.; Zhao, H. -Y.; Yang, X. -Y.; Lei, H.; Xin, M.; Cao, Y.-X.; Zhang, S. -Q. *Bioorg. Med. Chem.* **2018**, *26*, 3619.
4. Kissova, M.; Maga, G.; Crespan, E. *Bioorg. Med. Chem.* **2016**, *24*, 4555.
5. Ban,H. S.; Tanaka, Y.; Nabeyama, W.; Hatori, M.; Nakamura, H. *Bioorg. Med. Chem.* **2010**, *18*, 870.
6. Wang, M.; Xu, S.; Lei, H.; Wang, C.; Xiao, Z.; Jia, S.; Zhi, J.; Zheng, P.; Zhu, W. *Bioorg. Med. Chem.* **2017**, *25*, 5754.
7. Lu, W.; Li, P.; Shan, Y.; Su, P.; Wang, J.; Shi, Y.; Zhang, J. *Bioorg. Med. Chem.* **2015**, *23*, 1044.
8. Gangjee, A.; Zhao, Y.; Raghavan, S.; Ihnat, M. A.; Disch, B. C. *Bioorg. Med. Chem.* **2010**, *18*, 5261.
9. Lin, W. H.; Hsu, J. T.; Hsieh, S. Y.; Chen, C. T.; Song, J. S.; Yen, S. C.; Hsu, T.; Lu, C. T.; Chen, C. H.; Chou, L. H.; Yang, Y. N.; Chiu, C. H.; Chen, C. P.; Tseng, Y. J.; Yen, K. J.; Yeh, C. F.; Chao, Y. S.; Yeh, T. K.; Jiaang, W. T. *Bioorg. Med. Chem.* **2013**, *21*, 2856.
10. Ravez, S.; Arsenlis, S.; Barczyk ,A.; Dupont, A.; Frédérick, R.; Hesse, S.; Kirsch, G.; Depreux, P.; Goossens, L. *Bioorg. Med. Chem.* **2015**, *23*, 7340.
11. Machado, V. A.; Peixoto, D.; Costa, R.; Froufe, H. J.; Calhelha, R. C.; Abreu, R. M.; Ferreira, I. C.; Soares, R.; Queiroz, M. J. *Bioorg. Med. Chem.* **2015**, *23*, 6497.
12. Albert, D. H.; Tapang, P.; Magoc, T. J.; Pease, L. J.; Reuter, D. R.; Wei, R. Q.; Li, J.; Guo, J.; Bousquet, P. F.; Ghoreishi-Haack, N. S.; Wang, B.; Bukofzer, G. T.; Wang, Y. C.; Stavropoulos, J. A.; Hartandi, K.; Niquette, A. L.; Soni, N.; Johnson, E. F.; McCall, J. O.; Bouska, J. J.; Luo, Y.; Donawho, C. K.; Dai, Y.; Marcotte, P. A.; Glaser, K. B.; Michaelides, M. R.; Davidsen, S. K. *Mol. Cancer Ther*. **2006**, *5*, 995.
13. Dai, Y.; Hartandi, K.; Ji, Z.; Ahmed, A. A.; Albert, D. H.; Bauch, J. L.; Bouska, J. J.; Bousquet, P. F.; Cunha, G. A.; Glaser, K. B.; Harris, C. M.; Hickman, D.; Guo, J.; Li, J.; Marcotte, P. A.; Marsh, K. C.; Moskey, M. D.; Martin, R. L.; Olson, A. M.; Osterling, D. J.; Pease, L. J.; Soni, N. B.; Stewart, K. D.; Stoll, V. S.; Tapang, P.; Reuter, D. R.; Davidsen, S. K.; Michaelides, M. R. *J. Med. Chem.* **2007**, *50*, 1584.
14. Lu, Y.; Mao, F.; Li, X.; Zheng, X.; Wang, M.; Xu, Q.; Zhu, J.; Li, J. *J. Med. Chem*. **2017**, *60*, 5099.
15. Wissner, A.; Fraser, H. L.; Ingalls, C. L.; Dushin, R. G.; Brawner Floyd, M.; Cheung, K.; Nittoli, T.; Ravi, M. R.; Tan, X.; Loganzo, F. *Bioorg. Med. Chem*. **2007**, *15*, 3635.

16. Solin, N.; Han, L.; Che, S.; Terasaki, O. *Catal. Commun*. **2009**, *10*, 1386.
17. Wang, Y.; Yuan, W.; Zheng, H. -F.; Shi, D. -Q. *Synthesis* **2013**, *45*, 382.
18. Miao, C. -B.; Wang, Y. -H.; Dong, C. -P. *Heterocycles*, **2013**, *87*, 2599.
19. Misic-Vukovic, M.; Jovanovic, S.; Mijin, D.; Csanadi, J.; Djokovic, D. *J. Serb. Chem. Soc.* **2007**, *72*, 1229.
20. Ma, C.; Jin, K.; Cao, J.; Zhang, L.; Li, X.; Xu, W. *Bioorg. Med. Chem.* **2013**, *21*, 1621.
21. Liu, D.; Tian, Z.; Yan, Z.; Wu, L.; Ma, Y.; Wang, Q.; Liu, W.; Zhou, H.; Yang, C. *Bioorg. Med. Chem.* **2013**, *21*, 2960.
22. Jöst, C.; Nitsche, C.; Scholz, T.; Roux, L.; Klein, C. D. *J. Med. Chem.* **2014**, *57*, 7590.
23. Cee, V. J.; Volak, L. P.; Chen, Y.; Bartberger, M. D.; Tegley, C.; Arvedson, T.; McCarter, J.; Tasker, A. S.; Fotsch, C. *J. Med. Chem.* **2015**, *58*, 9171.
24. Zhang, Y.; Chen, Y.; Zhang, D.; Wang, L.; Lu, T.; Jiao, Y. *J. Med. Chem.* **2018**, *61*, 140.
25. Park, H.-J.; Zhang, Y.; Georgescu, S. P.; Johnson, K. L.; Kong, D.; Galper, J. B. *Stem Cell Rev. Rep*. **2006**, *2*, 93.
26. Shan, Y.; Wang, C.; Zhang, L.; Wang, J.; Wang, M.; Dong, Y. *Bioorg. Med. Chem*. **2016**, *24*, 750.
27. Liu, Z.; Wang, L.; Feng, M.; Yi, Y.; Zhang, W.; Liu, W.; Li, L.; Liu, Z.; Li, Y.; Ma, X. *Bioorg. Chem.* **2018**, *77*, 593.
28. Prime, M. E.; Andersen, O. A.; Barker, J. J.; Brooks, M. A.; Cheng, R. K.; Toogood-Johnson, I.; Courtney, S. M.; Brookfield, F. A.; Yarnold, C. J.; Marston, R. W.; Johnson, P. D.; Johnsen, S. F.; Palfrey, J. J.; Vaidya, D.; Erfan, S.; Ichihara, O.; Felicetti, B.; Palan, S.; Pedret-Dunn, A.; Schaertl, S.; Sternberger, I.; Ebneth, A.; Scheel, A.; Winkler, D.; Toledo-Sherman, L.; Beconi, M.; Macdonald, D.; Muñoz-Sanjuan, I.; Dominguez, C.; Wityak, J. *J. Med. Chem.* **2012**, *55*, 1021.
29. Tardieu, J.-L. *Nat. Methods* **2007**, *4*, i.
30. Song, Z.-L.; Wang, M.-J.; Li, L.; Wu, D.; Wang, Y.-H.; Yan, L.-T.; Morris-Natschke, S. L.; Liu, Y.-Q.; Zhao, Y.-L.; Wang, C.-Y.; Liu, H.; Goto, M.; Liu, H.; Zhu, G.-X.; Lee, K.-H. *Eur. J. Med. Chem*. **2016**, *115*, 109.

Design, synthesis and structure-activity relationship of diaryl-ureas with novel isoxazol[3,4-*b*]pyridine-3-amino-structure as multi-target inhibitors against receptor tyrosine kinase

Zhi-Hao Shi[a], Feng-Tao Liu[a], Hao-Zhong Tian[a], Yan-Min Zhang[a], Nian-Guang Li[b,*], Tao Lu[a,*]

[a]School of Science, China Pharmaceutical University, 639 Longmian Avenue, Nanjing, Jiangsu 211198, China

[b]National and Local Collaborative Engineering Center of Chinese Medicinal Resources Industrialization and Formulae Innovative Medicine, Nanjing University of Chinese Medicine, 138 Xianlin Road, Nanjing, Jiangsu 210023, China

* Corresponding author.

E-mail addresses: linianguang@njutcm.edu.cn (N.-G. Li), lutao@cpu.edu.cn (T. L)

Graphical abstract